Cell Membrane Tethers Generate Mechanical Force in Response to Electrical Stimulation

William E. Brownell,[†‡*] Feng Qian,[‡] and Bahman Anvari[‡]
[†]Bobby R. Alford Department of Otolaryngology, Head & Neck Surgery, and Department of Neuroscience, Baylor College of Medicine, Houston, Texas; and [‡]Department of Bioengineering, Rice University, Houston, Texas

ABSTRACT Living cells maintain a huge transmembrane electric field across their membranes. This electric field exerts a force on the membrane because the membrane surfaces are highly charged. We have measured electromechanical force generation by cell membranes using optically trapped beads to detach the plasma membrane from the cytoskeleton and form long thin cylinders (tethers). Hyperpolarizing potentials increased and depolarizing potentials decreased the force required to pull a tether. The membrane tether force in response to sinusoidal voltage signals was a function of holding potential, tether diameter, and tether length. Membrane electromechanical force production can occur at speeds exceeding those of ATP-based protein motors. By harnessing the energy in the transmembrane electric field, cell membranes may contribute to processes as diverse as outer hair cell electromotility, ion channel gating, and transport.

INTRODUCTION

Cell membranes are soft ensembles of lipids, proteins, and other molecules. The proportions of the components vary but lipids dominate, reaching 10^2 lipid molecules for every protein in some membranes (1,2). They are very thin (typically ~5 nm) but cover large surface areas ($>10^3$ μm^2 in the case of the plasma membrane). Living cells expend metabolic energy to sustain electrochemical potentials (~100 mV) across their membranes, and the associated transmembrane electric field is large (>10 MV/m; compare to the ~3 MV/m fields associated with atmospheric lighting). Changes in the transmembrane electric field are biologically important signals. The action potential is a particularly dramatic example because the field which points into the cell at rest transiently reverses direction.

Living cells also expend energy to maintain a characteristic asymmetry in the number of lipid-associated fixed charges on the inner and outer surfaces of their membranes (3) where the inner surface is typically more negatively charged than the outer. Integral membrane proteins can contribute to the electrical charge difference at the two surfaces. The charge asymmetry of the membrane gives rise to an intrinsic electrical polarization that sets the stage for a piezoelectric-like force generation. The electrical and mechanical properties of membranes have been studied separately for many years; the interplay between the two has only been recently explored.

The first indirect evidence that biological membrane mechanics was influenced by the transmembrane potential difference came from the modulation of membrane birefringence associated with changes in membrane potential (4). Further evidence for electrically active membranes came from experiments that measured electromechanical force in axons (5–7), mammalian outer hair cells (8), purple membranes (9), and in cultured mammalian cells (10–13). Voltage-dependent lipid lateral diffusion in the plasma membrane of outer hair cells (14) is another likely manifestation of membrane electromechanics. Because the membrane of living cells is attached to the cytoskeleton, the direct contribution of the membrane in these early experiments could only be inferred. However, nonbiological bilayer (or black) lipid membranes that do not contain proteins were shown to bend in response to changes in the transmembrane potential (15).

We have combined optical tweezers and patch-clamp techniques (Fig. 1) for the purpose of pulling membrane tethers from a cell under whole-cell voltage-clamped conditions (16,17). The mechanical response of the tether to constant or modulated transmembrane electrical fields is measured. We observe a robust electromechanical response by membrane tethers pulled from outer hair cells (OHC) and human embryonic kidney (HEK) cells.

MATERIALS AND METHODS

Optical tweezer/patch-clamp setup

The mechanical properties of cell membranes have been examined by using micropipettes or trapped beads to separate the membrane from the cytoskeleton and deform it under controlled conditions (18–26). We combined optical tweezers with voltage-clamp to measure mechanical force produced by the tether in response to changes in the transmembrane potential difference. Our apparatus was configured around an inverted microscope (Axiovert S100TV; Zeiss, Oberkochen, Germany) and has been previously described (16). The trapping beam was a continuous wave, tunable (650–1100 nm) Titanium-Sapphire laser (3900S; Spectra-Physics, Santa Clara, CA) pumped by a 5 W solid-state Nd:YVO_4 laser (Millennia V; Spectra-Physics), operated at 830 nm. Laser power was set so that the trapping force was greater than the tether formation force. The trapping

Submitted October 22, 2009, and accepted for publication May 10, 2010.

*Correspondence: brownell@bcm.tmc.edu

Feng Qian's and Bahman Anvari's present address is the Department of Bioengineering, University of California, Riverside, CA, 92521-0144.

Editor: Edward H. Egelman.

0006-3495/10/08/0845/8 $2.00

doi: 10.1016/j.bpj.2010.05.025

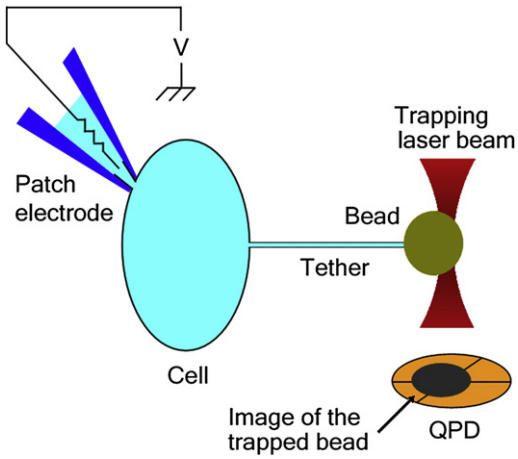

FIGURE 1 Experimental setup. Schematic of membrane tether formation with optical tweezer and electrical stimulation. Both constant and sinusoidal electrical stimuli are delivered to the cell through the whole-cell tight-seal patch electrode. Electromechanical force (F_{EM}) was quantified by measuring the bead displacements along the tether axis using the quadrant photodetector (QPD).

stiffness was at least three times the OHC tether stiffness (21). The laser beam was focused by a 100×, high numerical-aperture (NA = 1.3) oil-immersion objective (Plan-Neofluar; Zeiss). A charge-coupled device camera (CCD100; DAGE-MTI, Michigan City, IN) was used for visualization of the objects, and a quadrant photodetector (QPD) (S1557; Hamamatsu, Hamamatsu City, Japan) for position sensing of trapped beads.

Polystyrene beads with a diameter of 4.5 μm (cat. No. 17135; Polysciences, Niles, IL) were used to pull membrane tethers from cells. Under microscope bright-field illumination, the shadow of the trapped bead was projected onto the QPD active area. The differential signals (in mV) from the QPD sum-and-difference amplifier (QP50-6SD; Pacific Silicon Sensor, Westlake Village, CA) were digitized with an analog-to-digital converter (Wavebook 512; IOTech, Cleveland, OH), and subsequently recorded by LabVIEW (Ver. 6.0; National Instruments, Austin, TX) or WaveView software (WaveView 7.14.16; IOTech). The data acquisition rate was 1 kHz for signals with a frequency <100 Hz; for higher frequencies, it was 25 kHz. The QPD signal represented the displacement of the bead position from the trapping center, which was proportional to an external force (in pN) experienced by the bead. The trapping stiffness (in pN/mV) was calibrated by the viscous drag force method utilizing Stokes' Law (see Supporting Material), in which a known drag force was applied to the trapped bead while recording the resulting differential voltage signals from the QPD. The drag force was generated by driving a piezoelectric translation stage (P-527.3CL; Physik Instrumente, Auburn, MA) at known velocities. Resolution of the piezoelectric stage at the x,y plane was 2 nm.

Once an optically trapped bead was placed in contact with the cell, the tether was formed and elongated by moving the cell away from the trapped bead at a preset velocity. The movement trajectory was controlled by a function generator (DS345; Stanford Research Systems, Sunnyvale, CA). To avoid differential movements between the patch electrode and the voltage-clamped cells during the tether elongation, a compact micromanipulator was mounted on the piezoelectric stage to ensure simultaneous movement of the electrode and cell (16). When the bead is separated from the cell, the membrane detaches from the underlying cytoskeleton and forms a long, thin cylindrical membrane tube. Integral membrane proteins have been shown to flow into membrane tethers from red blood cells (27). OHC tethers do not contain f-actin (22). For HEK cells, our measurements were made before f-actin could polymerize in the tethers as evidenced by the observation that the tethers retracted back to the cell body rapidly once the trapped force was released (28). After polymerization begins, the new cytoskeletal filaments formed in the tethered region would prevent a complete retraction of the tether. The data presented in this article were obtained from single tethers. In the case of HEK cells, ~20% of the successful tether formations resulted in multiple tethers that could be visualized (see Fig. S1 in the Supporting Material) consistent with previous reports (29). The peak and steady-state forces associated with the multiple tethers were either two or three times those of single tethers. We calculated a single tether force from the multiple tethers by dividing by two or three, based on morphology. The mean and distribution of the calculated forces were indistinguishable from morphologically confirmed single tether data.

Cell preparations

HEK cells (HEK293) were seeded on a microwell petri dish at concentrations of ~15,000 per microwell area. The cells were maintained at 37°C within Dulbecco's modified Eagle's medium (Invitrogen Life Technologies, Carlsbad, CA) supplemented with 10% fetal bovine serum (Invitrogen Life Technologies) for at least 3 h to ensure firm attachment of the cells to a poly-*d*-lysine-coated coverslip.

Guinea pigs of either sex weighing 200–250 g were decapitated following a protocol approved by the Baylor College of Medicine (Houston, TX). The organ of Corti was isolated from the cochlea, incubated for 10 min with 0.5 mg/mL trypsin, and dissociated onto a microwell petri dish. OHCs were selected for experimentation if they exhibited a uniformly cylindrical shape, a basally located nucleus, and showed only limited osmotic swelling and/or Brownian motion in the cytoplasm. All OHCs were used within 3 h after animal sacrifice.

Electrophysiology

Cells were bathed in an ion-channel-blocking saline consisting of 100 mM NaCl, 20 mM CsCl, 20 mM tetraethylammonium, 10 mM HEPES, 2 mM $CoCl_2$, 1.47 mM $MgCl_2$, and 2 mM $CaCl_2$. For HEK cells, 1 μM Na^+ channel blocker Tetrodotoxin (T5651; Sigma, St. Louis, MO) was also added to the bath saline. Patch electrodes with typical resistances of 2–3 MΩ were pulled from borosilicate capillary tubing (TW100-4; World Precision Instruments, Sarasota, FL) with a carbon dioxide laser puller (P-2000; Sutter Instruments, Novato, CA). The patch electrodes contained 140 mM CsCl, 1 mM EGTA, 2 mM $MgCl_2$, and 10 mM HEPES. The solutions were adjusted to a pH of 7.2–7.3 using 1 M CsOH and an osmolality of 295–305 mOsm/kg using glucose. Electrophysiological recordings were performed under whole-cell configuration with a patch-clamp amplifier (Axopatch 200B; Axon Instruments, Foster City, CA). Voltage stimulus protocols and whole-cell current recording were made using pCLAMP 9.0 software (Axon Instruments). To avoid electrical coupling among HEK cells as a result of gap junctions, only isolated cells were used. The initial membrane resistance for HEK cells and OHCs were >500 MΩ and 150 MΩ, respectively, with series resistance <10 MΩ. The data-acquisition programs also recorded the voltage stimulation signals from the patch-clamp amplifier to synchronize the transmembrane voltage and the resulting electromechanical force of the membrane tethers. All experiments were performed at room temperature (21–23°C).

Membrane tether imaging

Membrane tethers were imaged using bright-field microscopy (Fig. 2; see also Fig. 6 *A* and Fig. S1). Images were detected with the charge-coupled device camera. We typically see faint shadows representing tethers pulled from HEK cells. Multiple images of the same tether were averaged and background-subtracted to produce the images.

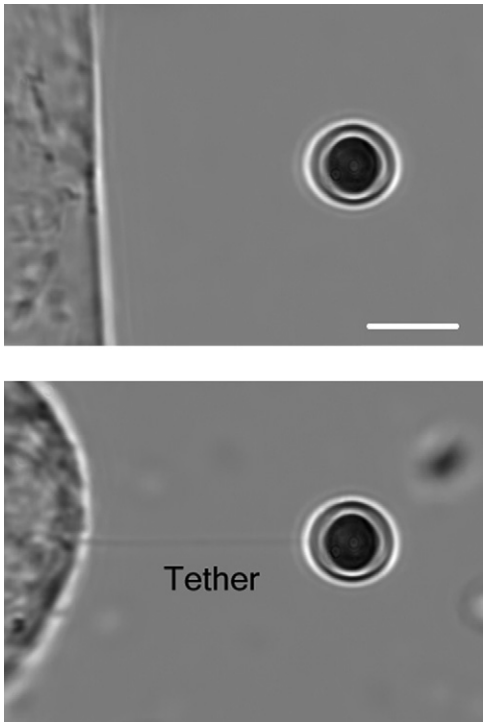

FIGURE 2 Photomicrographs of OHC (*top*) and HEK (*bottom*) cells connected to trapped beads by membrane tethers. The HEK tether is visible but OHC tethers were too narrow to be resolved. Scale bar = 5 μm.

RESULTS

Tether dimensions

Membrane tethers are characterized by their high curvature (0.002 ~ 0.02 nm^{-1}). Tethers pulled from OHCs had diameters that were smaller than the optical resolution of our system whereas tethers pulled from HEK cells could be visualized. (Fig. 2). OHC tethers had a larger tether formation force (the force required to bend and separate the membrane from the cytoskeleton) and their steady-state force (asymptotic force relaxation after tether elongation and maintaining a nearly-fixed length) was greater than that of HEK tethers (as previously reported for non-voltage-clamped cells (21)). Tethers from either cell type could be pulled to lengths in excess of 100 μm without breaking. A 30-μm-long tether with a radius of 100 nm would have a surface area of ~19 μm^2. If the radius is 75 nm, the surface area is ~14 μm^2. The microscopic surface area of a 50–75-μm-long OHC (not including the stereocilia) is between 2000 and 2500 μm^2 (30). OHCs have an ~10% excess surface area arising from nanoscale folding of the membrane (31). The membrane capacitance of the HEK cells indicates a surface area comparable to that of OHCs. A 30-μm tether therefore represents somewhere between 0.5 and 1.0% of the surface area of either cell type.

Peak and steady-state tether forces vary with the holding potential

The effect of a change in the transmembrane electric field on the membrane tether force was examined by measuring the force required to form and maintain tethers at different holding potentials. Fig. 3 shows typical tether force profiles at two different holding potentials. The electric field across the membrane affected the mechanical force required to pull and maintain the HEK plasma membrane tether, with hyperpolarizing potentials resulting in greater tether force.

Sinusoidal electric fields generate a sinusoidally modulated electromechanical force

The effect of modulating the transmembrane electric field on tether force generation was determined by applying a sinusoidal electrical stimulus after the tether force reached steady state (Fig. 4 *A*, Fig. S2, and Movie S1). Stimulation with a sinusoidal waveform generated an electromechanical force (F_{EM}) such that hyperpolarization relative to the holding potential increased and depolarization decreased the force exerted by the tether. In Fig. 4 *A*, the electromechanical gain (~0.3 pN/mV) measured for the OHC tether was ~5 times that of the HEK tether. The F_{EM} generated by a membrane tether also tracks electrical stimuli through acoustic frequencies as shown in Fig. 4 *B*, where the Fourier spectra peak of the F_{EM} generated by three different membrane tethers relative to that of the OHC tether is presented. The OHC F_{EM} was ~6 times that of the HEK F_{EM}.

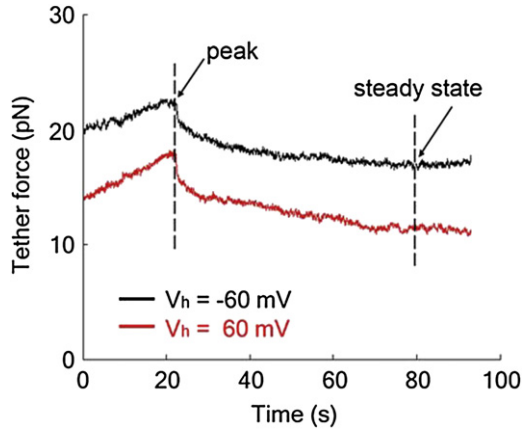

FIGURE 3 Representative tether force profiles plotted against time for tethers from two HEK cells at −60 mV (*black trace*) and 60 mV (*red trace*) holding potentials. Membrane tethers were pulled at a constant rate of 1 μm/s to a 30-μm length; note that the force profiles begin (time zero) when the tethers have reached a length of 10 μm. For a population of cells held at –60 mV ($n = 12$), the peak force (value at the end of elongation) was 24.5 ± 2.8 pN (mean ± SE) and the steady-state force was 16.4 ± 4.1 pN. Another population was depolarized to 60 mV ($n = 9$), the peak force was 18.4 ± 3.2 pN, and the steady-state force was 8.7 ± 2.9 pN. The force values at the two holding potentials are significantly different ($p < 0.001$, unpaired Student's *t*-test).

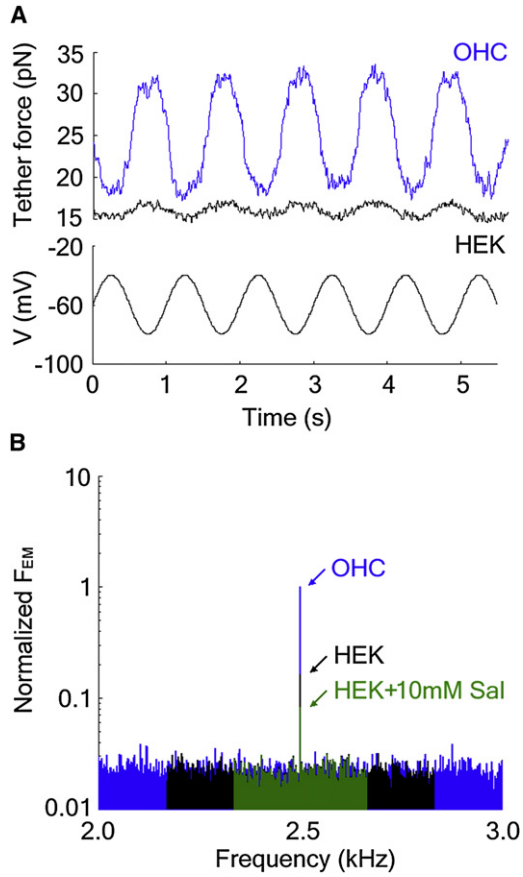

FIGURE 4 Effect of changing the transmembrane electric field on tether force generation (F_{EM}) by 30-μm-long tethers. (*A*) F_{EM} generated by membrane tethers (*top two traces*) in response to 1 Hz sinusoidal stimulation (*bottom trace*). (*B*) Representative F_{EM} of OHC (*blue*), HEK (*black*), and HEK + 10 mM salicylate (*green*) tethers is shown in response to a sinusoidal voltage signal ($\pm$20 mV, 2.5 kHz) riding on a –60 mV holding potential. The traces have been normalized to the OHC peak value (0.49 pN—an underestimate, see Supporting Material). The diameter of the HEK tether is larger than the OHC tether (see Fig. 2).

Salicylate is the anionic amphipathic metabolite of aspirin. It induces hearing loss by blocking the membrane-based motor mechanism responsible for OHC electromotility. Addition of 10 mM salicylate to the bathing solution decreased the HEK F_{EM} by ~50%.

The amplitude of F_{EM} decreased with increasing frequency because of electrical and mechanical low-pass filtering. Viscous damping acting on the bead attenuates bead displacements as the frequency increases (see Fig. S7). In addition to viscous damping effects on the bead, low-pass filtering of the electrical stimulus also attenuates the response at high frequencies. There are two sources of electrical filtering:

1. The high impedance head stage of the patch-clamp amplifier, and
2. The electrical properties of the cell membrane.

The two sources contribute to a global time constant of ~5 ms. Nevertheless, we have observed F_{EM} above the noise floor as high as 4 kHz for HEK and 10 kHz for OHC tethers.

F_{EM} varies with holding potential

F_{EM} was measured at five holding potentials for two populations of HEK cell tethers stimulated at 1 kHz, one population in normal saline and the other in 10 mM salicylate, as well as OHC tethers stimulated at 6 Hz. The five holding potentials were −120 mV, −60 mV, 0 mV, 60 mV, and 120 mV (see Fig S4 *a* for protocol). F_{EM} values at each holding potential were normalized to the F_{EM} at 0 mV for each measurement. Hyperpolarization of the holding potentials resulted in an increase in the amplitude of the tether's F_{EM} and depolarization decreased the F_{EM} (Fig. 5 *A*). The F_{EM} was largest at –120 mV holding potential and was reduced by a factor of three as the membrane became increasingly depolarized. Exposure to salicylate diminished

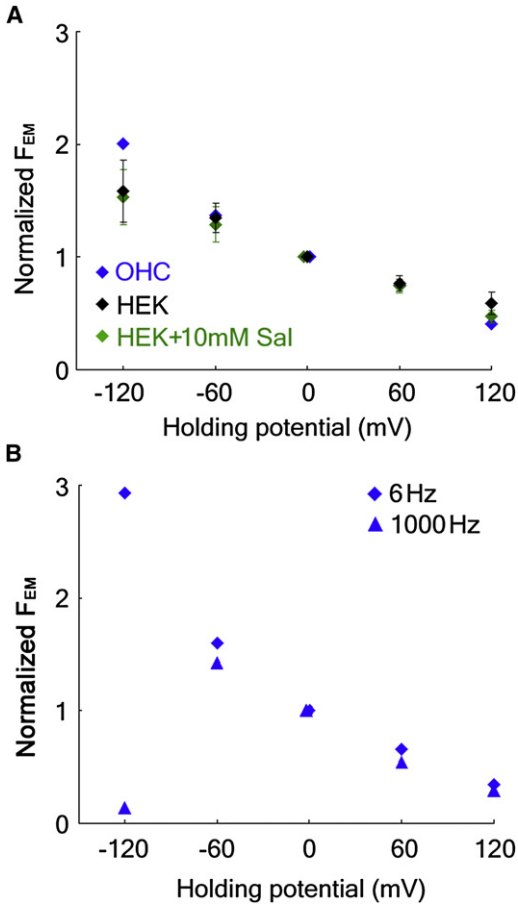

FIGURE 5 Effect of changing the holding potential on F_{EM}. (*A*) Average F_{EM} and standard error (SE) for two populations of HEK cell tethers stimulated at 1 kHz, one population in normal saline, and the other in 10 mM salicylate, as well as average F_{EM} for OHC tethers stimulated at 6 Hz. (*B*) F_{EM} as a function of holding potential for an OHC tether at 6 Hz and 1 kHz. The forces in panels *A* and *B* have been normalized to the value obtained at zero mV holding potential.

the F_{EM} but the relative change in magnitude with the holding potential remained virtually identical to the untreated HEK cell (~–0.45%/mV). The mean absolute values for the three populations at 0 mV were 7.2 pN, 0.08 pN, and 0.04 pN for the OHC, HEK, and (HEK + Sal) populations, respectively (the HEK values are underestimates). If the population steady-state forces for the two holding potentials in Fig. 3 are normalized to the linearly interpolated value at 0 mV, the slope is similar at –0.51%/mV.

We found nearly identical relative changes in F_{EM} with holding potential in OHC tethers stimulated at 6 Hz. The normalized F_{EM} plot for three OHCs at 6 Hz overlay the normalized data for the HEK and HEK + salicylate cells (Fig. 5 *B*). However, stimulating OHC tethers at 1 kHz and normalizing the F_{EM} to the value generated at 0 mV resulted in lower values at –120 mV. The four remaining values overlay those for the HEK cells. Absolute values for 6 Hz and 1 kHz at 0 mV were 6.8 pN and 0.55 pN, respectively.

F_{EM} is dependent on tether diameter

To test the effect of changes in tether diameter on F_{EM}, we monitored F_{EM} while increasing tether length. Morphometric analysis of tether diameter in non-voltage-clamped HEK cells revealed that increases in the steady-state tether force were accompanied by decreases in tether diameter (Fig. 6 *A*, *insets*). Representative force profiles from HEK tethers in response to sinusoidal electrical stimulation and tether elongation are shown in Fig. 6, *A* and *B*. The force attained a local maximum when the tether reached the new length and was followed by a decline during which the tether force relaxed. The force profile at each length was qualitatively the same as those shown in Fig. 3. A 1 kHz sinusoidal stimulus (±50 mV riding on a –60 mV holding potential) was applied when the tether force approached steady state for each length. The F_{EM} at the three different lengths is plotted in Fig. 6 *B*.

Similar length dependence for the F_{EM} was observed while electrically stimulating as the tether was elongated (Fig. 6 *B*). The F_{EM} was measured continuously during the entire elongation with the same electrical stimulus as in Fig. 6 *A*. The pulling rate was 0.25 μm/s so that force relaxation kept up with increasing tether length. The values are normalized to the F_{EM} at 10 μm obtained by fitting with linear regression. The trend line is not shown. The phase of the response remained constant. The greater diameter of HEK tethers is consistent with their having a smaller tether force and F_{EM} than the OHC tethers. The fact that a smaller tether diameter is associated with a larger F_{EM} suggests the increase in F_{EM} observed with hyperpolarization (Fig. 5 *A*) may also be associated with a decrease in tether diameter.

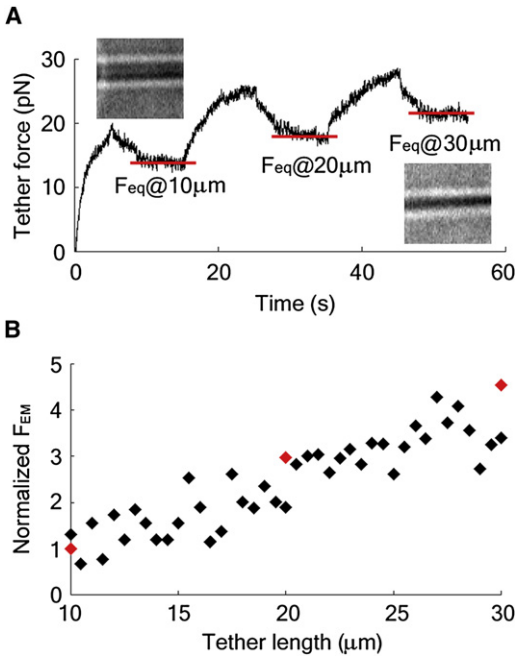

FIGURE 6 Effect of tether diameter on F_{EM}. (*A*) HEK tether force profile as the tether approached mechanical steady state (F_{eq}) for three different tether lengths. (*Insets*) Photomicrographs of the tether from another non-voltage-clamped HEK cell taken after steady-state forces were reached at 10 μm (*left inset*) and 30 μm (*right inset*). (*B*) The F_{EM} was measured continuously while the tether was elongated with the same electrical stimulus as in panel *A*. The three F_{EM} values measured at 10, 20, and 30 μm in panel *A* are plotted in red (normalized to the F_{EM} at 10 μm).

Cable properties

The frequency-dependent difference in F_{EM} at −120 mV (Fig. 5 *B*) suggests that the electrical cable properties of the 30-μm OHC tether were altered by changes in the holding potential such that hyperpolarization results in a decrease in the electrical length constant. A cable analysis of hair cell stereocilia (membrane nanotubes with dimensions similar to our experimental tethers) reveals that the low-pass corner frequency decreases as the tether diameter decreases (32). We have tested the changes in tether cable properties by monitoring the tether force and the F_{EM} as a function of tether length (Fig. 7 *A*). Low-pass filtering was also observed when the tether exceeded a specific length, because F_{EM} began to decrease after reaching a length-dependent peak. The monotonically increasing tether force is plotted as a continuous function of tether length and the F_{EM} is plotted every 1.8 μm between 10 μm and 60 μm (see Fig S4 *b* for protocol). The F_{EM} values are normalized to that at 10 μm obtained by the second-order polynomial fit (*dashed line*, $r^2 = 0.79$). The inflection point of the F_{EM} curve was at 37 μm. The phase remained nearly constant to the inflection point and showed an increasing phase lag thereafter. The decrease in F_{EM} after the inflection point most likely reflects the cable properties of the tether.

F_{EM} generated by an HEK cell tether was also measured at different lengths and frequencies. Fig. 7 *B* shows the results of voltage excitation at six frequencies (10, 50,

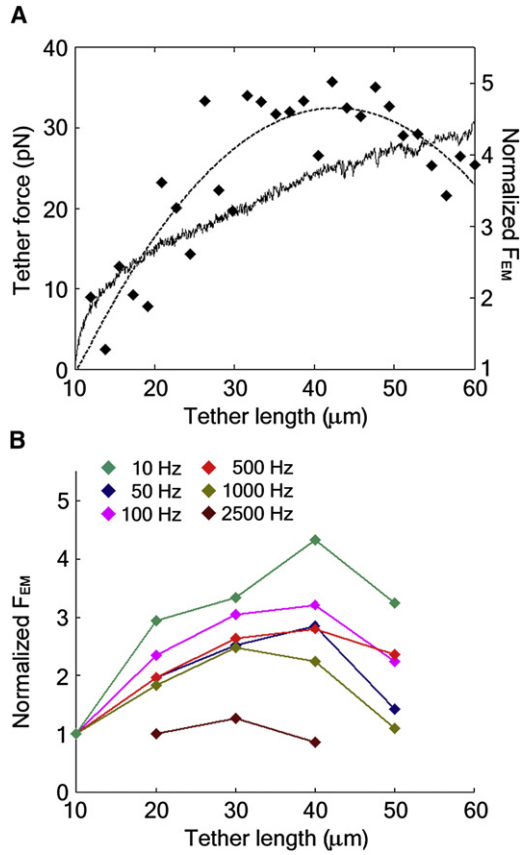

FIGURE 7 Tether cable properties affect F_{EM}. (*A*) The monotonically increasing tether force is plotted as a continuous function of tether length and the normalized F_{EM} (◆) is plotted every 1.8 μm between 10 μm and 60 μm. (*B*) F_{EM} generated by an HEK cell tether at different lengths and frequencies. The results are normalized to the F_{EM} amplitude at the 10-μm length except for the 2.5 kHz values, which are normalized to the amplitude at 20 μm. The F_{EM} amplitude for 2.5 kHz was below the noise floor at the 10-μm and 50-μm lengths.

100, 500, 1000, and 2500 Hz) applied when a tether reached successive lengths of 10, 20, 30, 40, and 50 μm, respectively. The F_{EM} at each frequency increased at the beginning of tether elongation, and then decreased after reaching a peak. The behavior is consistent with low-pass filtering resulting from tether-associated cable properties.

DISCUSSION

Converse flexoelectricity

Electrically evoked tether force production is consistent with the converse flexoelectric effect. Membrane flexoelectricity is the change in electrical polarization that results from bending a membrane (2,33,34). Converse flexoelectricity describes a change in membrane curvature resulting from a change in the transmembrane potential (15). Several mechanisms may contribute to flexoelectricity including reorientation of electrical dipoles in membrane molecules and changes in the interfacial or surface tension on both sides of the membrane (2,35). The modulation of surface tension by an electric field was first described by Lippmann (36) and has recently been used in the design and fabrication of microfluidic motors (37). A transmembrane electric field increases surface tension on one side of the membrane while reducing it on the other (35). The ability of the tethers to follow electrical signals at >5 kHz is consistent with a piezoelectric-like process and eliminates mechanisms with slower kinetics. The increases in F_{EM} with tether length increase, are also consistent with a converse flexoelectric origin but not with a piezoelectric or Maxwell stress origin for the electromechanical coupling (38). Because membrane curvature in a tether is determined by a consideration of force equilibrium (39), our results suggest that this equilibrium in biological membranes must also include the contribution of electrically generated forces.

A converse flexoelectric origin for the tether F_{EM} opens the possibility that similar forces are produced in any highly curved biological membrane. Examples of highly curved biological membranes abound. Intercellular tunneling nanotubes (40) between adjacent HEK cells in culture have geometries resembling our tethers. Another example is the stereocilia of hair cells, which are typically 200 nm in diameter and resemble the cellular membrane tethers from HEK cells. The stereocilia bundle is known to produce voltage-dependent flicks (41), the voltage dependence of which is consistent with a flexoelectric model (42). Peripheral dendrites and dendritic spines have smaller radii (higher curvature) than HEK tethers, as do mitochondrial cristae, synaptic vesicles, and membrane fusion pores (43). Dendritic spines, synaptic vesicles, and membrane fusion pores are all structures that might be able to utilize the change in energy in the transmembrane electric field during an action potential to modulate membrane mechanics. Finally, the crenellated membrane of the OHC displays high curvature and mechanical coupling with the cell's cytoskeleton that can explain the mechanical force underlying OHC electromotility (44).

Voltage sensing by membranes

Modulation of the transmembrane electric field should exert a force on the charged portions of voltage-gated ion channels. The magnitude of this force is the product of the transmembrane electric field, times the charge being moved ($F = (V/h)^{*}q$). There are four elementary charges per monomer in a voltage-gated potassium channel and the channel is a tetramer, so that total force would be ~0.3 pN if all the charges were equally influenced by the field produced by a 40-mV potential difference across a 5-nm-thick membrane. This is a small force that could be augmented by local bending of the membrane. It is possible that electrical dipoles in channel protein are influenced by the field, with the resulting torsion contributing to a converse flexoelectric response (bending) of the membrane. Local bending has

been considered as a mechanism that could contribute to ion-channel gating (45–49). A role for membrane mechanics in channel gating is supported by the fact that the kinetics of a variety of voltage-gated ion channels are modulated by membrane tension (50,51). The lipid composition of the membrane also affects voltage sensing (52), and coarse-grain molecular dynamic simulations suggest that the channel should locally deform the membrane (53). It is possible that the conformation change that opens and closes voltage-gated ion channels benefits from the ability of the membrane surrounding the protein to sense the transmembrane electric field, and deform.

Prestin and other members of the Slc26A family of anion transporters

The membrane protein prestin in the OHC lateral wall modifies membrane electromechanics. HEK membranes with prestin show a modest increase (2–3×) in force production over those without it (10,17). On the other hand, there is more than a three-order-of-magnitude increase in charge movement (54,55). Prestin's strong impact on charge movement most likely reflects its membership in the Slc26A family of anion transporters.

There are two reasons why transport molecules might benefit from flexoelectric membrane bending:

The first is that membrane bending leads to a differential tension between the leaflets of the bilayer, which could facilitate the conformational changes of the protein (45,47,49). In the case of prestin, the resulting electrodiffusion of anions into the resulting protein cavity can contribute to the measured charge movement (56).

A second benefit derives from the acoustic wave produced by the bending membrane. The resulting nanosonication would serve to mix the unstirred layer (57,58) and further facilitate transport. These considerations suggest that the origins of OHC electromotility may be linked to evolutionarily ancient mechanisms associated with membrane transport.

CONCLUSIONS

We have the following findings:

- Biological membranes are capable of electromechanical signaling and perform work in response to changes in the transmembrane electric field.
- The mechanical properties of the membrane that determine the force required to pull and maintain membrane tether are a function of the transmembrane electric field.
- The frequency limit for electromechanical signaling is >5 kHz.
- The magnitude of the electromechanical force is a function of the voltage-clamp holding-potential and membrane curvature.

SUPPORTING MATERIAL

Seven figures, one equation, and one movie are available at http://www.biophysj.org/biophysj/supplemental/S0006-3495(10)00662-4.

W.E.B. and B.A. conceived the project, W.E.B., F.Q., and B.A. contributed to the experimental design, F.Q. performed all the experiments, and W.E.B. and B.A. wrote the manuscript. We thank Drs. B. Farrell, H. Huang, C. E. Morris, A. G. Petrov, A. S. Popel, R. Rabbitt, R. Raphael, F. Sachs, and A. A. Spector for stimulating discussions, and C. D. Shope for technical assistance with the experiments.

This work was supported by a research grant from the National Institute of Deafness and other Communication Disorders at the National Institutes of Health (No. R01 DC02775 to W.E.B. and B.A.), a grant from the National Science Foundation (No. BES-0522862 to B.A.), a fellowship from the Keck Center Nanobiology Training Program of the Gulf Coast Consortia funded by the National Institutes of Health (No.1 R90 DK071504-01 to F.Q.), and the Jake and Nina Kamin Chair of Otorhinolaryngology (to W.E.B.).

REFERENCES

1. Dowhan, W., M. Bogdanov, and E. Mileykowskaya. 2008. Functional roles of lipids in membranes. *In* Biochemistry of Lipids, Lipoproteins and Membranes. D. E. Vance and J. E. Vance, editors. Elsevier B.V. Dordrecht, The Netherlands.
2. Sachs, F., W. E. Brownell, and A. G. Petrov. 2009. Membrane electromechanics in biology, with a focus on hearing. *MRS Bull.* 34:665.
3. Daleke, D. L. 2003. Regulation of transbilayer plasma membrane phospholipid asymmetry. *J. Lipid Res.* 44:233–242.
4. Cohen, L. B., R. D. Keynes, and B. Hille. 1968. Light scattering and birefringence changes during nerve activity. *Nature.* 218:438–441.
5. Iwasa, K., and I. Tasaki. 1980. Mechanical changes in squid giant axons associated with production of action potentials. *Biochem. Biophys. Res. Commun.* 95:1328–1331.
6. Terakawa, S. 1983. Changes in intracellular pressure in squid giant axons associated with production of action potentials. *Biochem. Biophys. Res. Commun.* 114:1006–1010.
7. Akkin, T., D. Landowne, and A. Sivaprakasam. 2009. Optical coherence tomography phase measurement of transient changes in squid giant axons during activity. *J. Membr. Biol.* 231:35–46.
8. Brownell, W. E., C. R. Bader, …, Y. de Ribaupierre. 1985. Evoked mechanical responses of isolated cochlear outer hair cells. *Science.* 227:194–196.
9. Kietis, P., M. Vengris, and L. Valkunas. 2001. Electrical-to-mechanical coupling in purple membranes: membrane as electrostrictive medium. *Biophys. J.* 80:1631–1640.
10. Ludwig, J., D. Oliver, …, B. Fakler. 2001. Reciprocal electromechanical properties of rat prestin: the motor molecule from rat outer hair cells. *Proc. Natl. Acad. Sci. USA.* 98:4178–4183.
11. Mosbacher, J., M. Langer, …, F. Sachs. 1998. Voltage-dependent membrane displacements measured by atomic force microscopy. *J. Gen. Physiol.* 111:65–74.
12. Zhang, P. C., A. M. Keleshian, and F. Sachs. 2001. Voltage-induced membrane movement. *Nature.* 413:428–432.
13. Zheng, J., W. Shen, …, P. Dallos. 2000. Prestin is the motor protein of cochlear outer hair cells. *Nature.* 405:149–155.
14. Oghalai, J. S., H. B. Zhao, …, W. E. Brownell. 2000. Voltage- and tension-dependent lipid mobility in the outer hair cell plasma membrane. *Science.* 287:658–661.
15. Todorov, A. T., A. G. Petrov, and J. H. Fendler. 1994. First observation of the converse flexoelectric effect in bilayer-lipid membranes. *J. Phys. Chem.* 98:3076–3079.

16. Qian, F., S. Ermilov, …, B. Anvari. 2004. Combining optical tweezers and patch clamp for studies of cell membrane electromechanics. *Rev. Sci. Instrum.* 75:2937–2942.

17. Zhang, R., F. Qian, …, B. Anvari. 2007. Prestin modulates mechanics and electromechanical force of the plasma membrane. *Biophys. J.* 93:L07–L09.

18. Cuvelier, D., N. Chiaruttini, …, P. Nassoy. 2005. Pulling long tubes from firmly adhered vesicles. *Europhys. Lett.* 71:1015–1021.

19. Dai, J., and M. P. Sheetz. 1999. Membrane tether formation from blebbing cells. *Biophys. J.* 77:3363–3370.

20. Ermilov, S. A., D. R. Murdock, …, B. Anvari. 2005. Effects of salicylate on plasma membrane mechanics. *J. Neurophysiol.* 94: 2105–2110.

21. Li, Z., B. Anvari, …, W. E. Brownell. 2002. Membrane tether formation from outer hair cells with optical tweezers. *Biophys. J.* 82: 1386–1395.

22. Oghalai, J. S., A. A. Patel, …, W. E. Brownell. 1998. Fluorescence-imaged microdeformation of the outer hair cell lateral wall. *J. Neurosci.* 18:48–58.

23. Sheetz, M. P. 2001. Cell control by membrane-cytoskeleton adhesion. *Nat. Rev. Mol. Cell Biol.* 2:392–396.

24. Sit, P. S., A. A. Spector, …, W. E. Brownell. 1997. Micropipette aspiration on the outer hair cell lateral wall. *Biophys. J.* 72:2812–2819.

25. Hochmuth, R. M., H. C. Wiles, …, J. T. McCown. 1982. Extensional flow of erythrocyte membrane from cell body to elastic tether. II. Experiment. *Biophys. J.* 39:83–89.

26. Marcus, W. D., and R. M. Hochmuth. 2002. Experimental studies of membrane tethers formed from human neutrophils. *Ann. Biomed. Eng.* 30:1273–1280.

27. Berk, D. A., and R. M. Hochmuth. 1992. Lateral mobility of integral proteins in red blood cell tethers. *Biophys. J.* 61:9–18.

28. Zhelev, D. V., and R. M. Hochmuth. 1995. Mechanically stimulated cytoskeleton rearrangement and cortical contraction in human neutrophils. *Biophys. J.* 68:2004–2014.

29. Xu, G., and J. Y. Shao. 2005. Double tether extraction from human neutrophils and its comparison with CD^{4+} T-lymphocytes. *Biophys. J.* 88:661–669.

30. Chertoff, M. E., and W. E. Brownell. 1994. Characterization of cochlear outer hair cell turgor. *Am. J. Physiol.* 266:C467–C479.

31. Morimoto, N., R. M. Raphael, …, W. E. Brownell. 2002. Excess plasma membrane and effects of ionic amphipaths on mechanics of outer hair cell lateral wall. *Am. J. Physiol. Cell Physiol.* 282: C1076–C1086.

32. Breneman, K. D., S. M. Highstein, …, R. D. Rabbitt. 2009. The passive cable properties of hair cell stereocilia and their contribution to somatic capacitance measurements. *Biophys. J.* 96:1–8.

33. Petrov, A. G., and P. N. Usherwood. 1994. Mechanosensitivity of cell membranes. Ion channels, lipid matrix and cytoskeleton. *Eur. Biophys. J.* 23:1–19.

34. Rey, A. D. 2006. Liquid crystal model of membrane flexoelectricity. *Phys. Rev. E Stat. Nonlin. Soft Matter Phys.* 74:011710.

35. Petrov, A. G. 2002. Flexoelectricity of model and living membranes. *Biochim. Biophys. Acta.* 1561:1–25.

36. Lippmann, M. G. 1875. Relation between electrical phenomena and capillaries [Relation entre les phenomenes electriques et capillaires]. *Ann. Chim. Phys.* 5:494–549.

37. Lee, J., and C. Kim. 2000. Surface-tension-driven microactuation based on continuous electrowetting. *J. Microelectromech. Syst.* 9:171–180.

38. Glassinger, E., A. C. Lee, and R. M. Raphael. 2005. Electromechanical effects on tether formation from lipid membranes: a theoretical analysis. *Phys. Rev. E Stat. Nonlin. Soft Matter Phys.* 72:041926.

39. Zimmerberg, J., and M. M. Kozlov. 2006. How proteins produce cellular membrane curvature. *Nat. Rev. Mol. Cell Biol.* 7:9–19.

40. Rustom, A., R. Saffrich, …, H. H. Gerdes. 2004. Nanotubular highways for intercellular organelle transport. *Science.* 303:1007–1010.

41. Cheung, E. L., and D. P. Corey. 2006. Ca^{2+} changes the force sensitivity of the hair-cell transduction channel. *Biophys. J.* 90:124–139.

42. Breneman, K. D., W. E. Brownell, and R. D. Rabbitt. 2009. Hair cell bundles: flexoelectric motors of the inner ear. *PLoS ONE.* 4:e5201.

43. McMahon, H. T., and J. L. Gallop. 2005. Membrane curvature and mechanisms of dynamic cell membrane remodeling. *Nature.* 438:590–596.

44. Raphael, R. M., A. S. Popel, and W. E. Brownell. 2000. A membrane bending model of outer hair cell electromotility. *Biophys. J.* 78: 2844–2862.

45. Lee, K. J. 2005. Effects of hydrophobic mismatch and spontaneous curvature on ion channel gating with a hinge. *Phys. Rev. E Stat. Nonlin. Soft Matter Phys.* 72:031917.

46. Lee, K. J. 2006. Energetics of rotational gating mechanisms of an ion channel induced by membrane deformation. *Phys. Rev. E Stat. Nonlin. Soft Matter Phys.* 73:021909.

47. Turner, M. S., and P. Sens. 2004. Gating-by-tilt of mechanically sensitive membrane channels. *Phys. Rev. Lett.* 93:118103.

48. Wiggins, P., and R. Phillips. 2004. Analytic models for mechanotransduction: gating a mechanosensitive channel. *Proc. Natl. Acad. Sci. USA.* 101:4071–4076.

49. Wiggins, P., and R. Phillips. 2005. Membrane-protein interactions in mechanosensitive channels. *Biophys. J.* 88:880–902.

50. Calabrese, B., I. V. Tabarean, …, C. E. Morris. 2002. Mechanosensitivity of N-type calcium channel currents. *Biophys. J.* 83:2560–2574.

51. Gu, C. X., P. F. Juranka, and C. E. Morris. 2001. Stretch-activation and stretch-inactivation of *Shaker*-IR, a voltage-gated K^+ channel. *Biophys. J.* 80:2678–2693.

52. Schmidt, D., Q. X. Jiang, and R. MacKinnon. 2006. Phospholipids and the origin of cationic gating charges in voltage sensors. *Nature.* 444:775–779.

53. Bond, P. J., and M. S. Sansom. 2007. Bilayer deformation by the Kv channel voltage sensor domain revealed by self-assembly simulations. *Proc. Natl. Acad. Sci. USA.* 104:2631–2636.

54. Brownell, W. E. 2006. The piezoelectric outer hair cell: bidirectional energy conversion in membranes. *In* Auditory Mechanisms: Processes and Models. A. L. Nuttall, P. Gillespie, T. Ren, K. Grosh, and E. de Boer, editors. World Scientific, Singapore.

55. Farrell, B., C. Do Shope, and W. E. Brownell. 2006. Voltage-dependent capacitance of human embryonic kidney cells. *Phys. Rev. E Stat. Nonlin. Soft Matter Phys.* 73:041930.

56. Sun, S. X., B. Farrell, …, A. A. Spector. 2009. Voltage and frequency dependence of prestin-associated charge transfer. *J. Theor. Biol.* 260:137–144.

57. Eisenberg, M., and S. McLaughlin. 1976. Lipid bilayers as models of biological membranes. *BioScience.* 26:436–443.

58. Finkelstein, A. 1987. Water Movement through Lipid Bilayers, Pores, and Plasma Membranes: Theory and Reality. Wiley Interscience, New York.